Available online at www.sciencedirect.com
ScienceDirect
International Journal of Mass Spectrometry 255–256 (2006) 177–184
International Journal of Mass Spectrometry
www.elsevier.com/locate/ijms

The unimolecular dissociation of protonated glyoxylic acid: Structure and dynamics of a step-by-step process

Osamu Sekiguchi [a], Matthias C. Letzel [b], Dietmar Kuck [b], Einar Uggerud [a,*]

[a] *Department of Chemistry, University of Oslo, P.O. Box 1033 Blindern, N-0315 Oslo, Norway*
[b] *University of Bielefeld, P.O. Box 100131, D-33501 Bielefeld, Germany*

Received 25 November 2005; received in revised form 27 December 2005; accepted 28 December 2005
Available online 7 February 2006

Dedicated to Diethard Bohme, who boldly goes where no one has gone before.

Abstract

The unimolecular chemistry of protonated glyoxylic acid $[HCOCOOH]H^+$, has been investigated by analyzing the fragmentation of metastable ions (MI) during their flight through a sector-field mass spectrometer. The only significant ionic product in the MI experiments is H_3O^+, indicating the loss of two carbon monoxide molecules. High-level ab initio calculations have been used to model the relevant parts of the potential energy surface (PES). Starting from the most stable isomer, $H(CO)C(OH)_2^+$ (**1**), fragmentation takes place as the result of three successive intramolecular proton transfer reactions. The first CO molecule is liberated in-between the second and the third proton transfer and moves slowly away. This mechanism is fully confirmed by ab initio direct dynamics calculations. In addition, the dynamics calculations reveal that the majority of the potential energy, which is liberated ends up as OH vibrations of the H_3O^+ moiety. After passage through the critical transition state, dissociation of the $H_2OH^+\cdots CO$ (**6**) complex appears to be a limiting step. In order to acquire sufficient relative translational energy to depart, the hydroxonium ion and carbon monoxide have to reside together for 1–2 ps.

Keywords: Mass spectrometry; Reaction dynamics; Reaction mechanism; Chemical ionization; Protonation; Ab initio; Quantum chemistry

1. Introduction

One fascinating aspect of studying the unimolecular decomposition of organic and bio-organic molecules is that the products often are simple molecules like CO, CO_2, CH_2O, H_2O and NH_3—species that are stable and abundant in many environments, both terrestrial and extraterrestrial. Identification of the fragments and their mode of formation may give clues to how the original molecules may be formed by synthesis or are actually made by nature, by applying the principle of microscopic reversibility. This retrosynthetic point of view has become evident through recent reports on the decomposition of the small protonated molecules: protonated glycine [1–4], protonated glycinamide [5], protonated formamide [6] and protonated formic acid [7], In this respect, the formation of amino acids and other biological molecules from small "inorganic" molecules is of particular interest in connection with how life may have evolved. However, one should of course realize that the existence of a unimolecular pathway for the dissociation of a more complex molecule into simpler constituents does not prove that the reverse process is an efficient way of producing the more complex molecule. To get insight into this possibility, detailed mapping of the relevant potential energy surface and describing the chemical reactions, as well as the reaction dynamics is important. To this end, both experiments and theoretical modelling are necessary.

One good example is protonated formic acid. Already in 1978, Mackay et al. [8] reported that proton transfer from H_3^+ to formic acid leads to two different ionic products, the hydroxonium ion and the formyl cation. Following up this important study, we were recently able to demonstrate how the detailed motion of the dissociating $HC(OH)_2^+$ molecule determines which product is formed [7]. After passing a common saddle point region a transient $HC(O)OH_2^+$ molecule is first formed. At high energies this transient species dissociates directly to give $HCO^+ + H_2O$, while at lower energies the life-time of

* Corresponding author. Tel.: +47 22855537; fax: +47 22855441.
E-mail address: einar.uggerud@kjemi.uio.no (E. Uggerud).

1387-3806/$ – see front matter © 2006 Elsevier B.V. All rights reserved.
doi:10.1016/j.ijms.2005.12.041

$HC(O)OH_2^+$ becomes sufficiently long for an intramolecular proton transfer from C to O, eventually producing $H_3O^+ + CO$.

The purpose of the present study is to extend the protonated formic acid $[HCOOH + H]^+$, study to protonated glyoxylic acid $[HCOCOOH + H]^+$—literally speaking, by adding one extra carbonyl group. One naïve idea is that this could be a suitable precursor for ethylenedione, OC=CO [9–11], since it has the OCCO motif built in. To us, however, it would be more interesting to see how the extra CO may alter the decomposition pattern in comparison to the native $[HCOOH + H]^+$, and the dynamics of the dissociation process. In order to study the reaction dynamics in more detail we wanted to employ mass-analyzed ion kinetic energy (MIKE) spectrometry and Fourier transform ion cyclotron resonance (FT-ICR) mass spectrometry. In addition, the reactions were modelled using ab initio direct dynamics calculations.

2. Experimental methods

The mass spectra were either recorded on a Fisons Autospec (EBE configuration), which runs at 8 kV for EI (electron energy 70 eV) and 6 kV for CI (electron energy 45 eV).

The precursor ion of interest was selected using the first two stages (EB). Ionic decomposition products were recorded in the third field free region, by scanning the second electric sector. For the 70 eV electron impact (EI) experiments the precursor ion was formed from 3,3,3-trifluorolactic acid. For chemical ionization (CI) a particularly tight ion source was used to ensure high-pressure conditions. Methane was used as the reagent gas in some of the protonation experiments, providing predominantly the proton donors CH_5^+ and $C_2H_5^+$ in approximately equal abundances, while a 1:1 mixture of hydrogen and carbon monoxide, which gives HCO^+ was used in other experiments. Collision-induced dissociation (CID) was achieved by allowing the selected precursor ions to collide with argon in the third field free region (after B). The argon pressure inside the collision cell was set to attenuate the intensity of the precursor ion peak to ca. 30%.

3. Theoretical methods

The relevant part of the $[H(CO)COOH + H]^+$ potential energy surface was first surveyed employing MP2/6–31 G(d,p) using the Gaussian 03 suite of programs [12]. All stationary points were subject to a complete geometry optimisation, including a check for the correct number of negative Hessian eigenvalues. At this stage, analytical force constants were computed and the vibrational harmonic frequencies were obtained together with the rotational constants. From these calculated spectroscopic constants, zero-point vibrational energies and thermochemical quantities were calculated within the rigid-rotor/harmonic-oscillator approximation. Zero-point vibrational energies were included with appropriate scaling factors [13]. The connectivity of a saddle point to reactant/product was checked by IRC calculations [14]. In addition, G3 theory [15] calculations were used to obtain the most accurate energy estimates. G3 theory is a compound technique, which involves initial geometry optimizations at the HF/6–31 G(d) level and subsequent calculation of zero point vibrational energies (ZPVEs) at the same level of theory. Then the geometry is re-optimized at the MP2 (full)/6–31 G(d) level whereupon a number of single-point MP2, MP4 and QCISD(T) calculations are performed in order to obtain an energy estimate which is effectively at the QCISD(T)/large level.

The direct ab initio approach to trajectory calculations utilizes the first and second derivatives of the electronic energy with respect to atomic displacements (gradients and Hessians) to generate molecular trajectories $\boldsymbol{q}(t) = \{\boldsymbol{q}(t_1), \boldsymbol{q}(t_2), \ldots\}$ within the Born–Oppenheimer approximation [16–19]. For efficiency, the trajectory is calculated using a fifth-order predictor–corrector method, based on the repeated calculation of the wave function and its geometrical derivatives at points $\boldsymbol{q}_i$ in time steps, typically varying between 0.2 and 0.5 fs. The energy and the molecular gradient are calculated at every point, whereas the Hessian is recalculated at every fifth point, being updated at the intermediate points. Each trajectory was calculated "on-the-fly" by a stepwise procedure calculating MP2 (fc)/6–31 G(d,p) wave functions at each point, starting from **TS(2′/3)** (vide infra). Vibrational and rotational degrees of freedom were sampled from ensembles at 298 K, respectively, and the transition mode was sampled thermally [20]. A total of 10 different trajectories were calculated.

4. Results and discussion

4.1. MI and CID experiments

Two sources of protonated glyoxylic acid (*m/z* 75) were used for the mass spectrometric investigations, namely chemical ionization (CI) of glyoxylic acid

$$AH^+ + HCOCOOH \rightarrow [HCOCOOH]H^+ + A \quad (A = CH_4 \text{ or } C_2H_4) \tag{1}$$

and electron ionization (EI) of 3,3,3-trifluorolactic acid

$$CF_3CHOHCOOH + e^- \rightarrow {}^+CHOHCOOH + CF_3 + 2e^- \tag{2}$$

Using methane CI (Eq. (1)), a strong ion signal at *m/z* 75 is observed. When the corresponding intense ion beam was subject to MI, however, very little fragment ion signal was observed. Extensive data collection gave a spectrum virtually identical to the corresponding CID spectrum, indicating that the observed fragmentation is collisionally induced rather than truly unimolecular. Greater success was achieved when a H_2/CO gas mixture was used to generate the CI plasma. In this plasma the dominating ion is HCO^+, which transfers less energy upon protonation to the molecules than CH_5^+, thereby providing ions $[HCOCOOH + H]^+$ with an internal energy probably close to the dissociation threshold. The spectrum is reproduced in Fig. 1. The most intense peak is at *m/z* 19, which we assign to the hydroxonium ion. In addition, there is a noticeable peak at *m/z* 29, and smaller peaks at *m/z* 45 and 46. All these are most likely collis-

sionally induced, since their relative amounts increase relative to *m/z* 19 with increasing gas pressure in the collision cell. On this basis we must conclude that the only secure observation of a truly unimolecular process is that leading to the ion with *m/z* 19. Use of EI of trifluorolactic acid as the precursor (Eq. (2)) gave some of the same problems as CI(CH_4) in terms of providing very few metastable ions. The yield of primary $C_2H_3O_3^+$ ions is rather meagre, in the sense that *m/z* 75 contributes to only a few percent of the total ion current. Correspondingly, the resulting MI spectrum is of rather low signal-to-noise ratio. However, the experimental observations support the results obtained by CI(H_2/CO). Again, the *m/z* 19 peak stands up as the significantly most intense signal, while no peaks with *m/z* 29, 45 and 46 could be seen in the spectrum. One complicating issue is that the observable signals at *m/z* 56 and 58 have to be considered artefact peaks, rather than being due to fragment ions from isobaric impurities of the primary ion beam. In fact, it was not possible to identify any such impurities even when the mass resolution was increased to $m/\Delta m = 1{,}800{,}000$ in an FI-ICR mass spectrometer. Tajima et al. have reported that the MIKE spectrum of *m/z* 75 produced from 3,3,3-trifluorolactic acid upon electron ionization shows only one peak at *m/z* 19 [21]. The CID spectra obtained for protonated glyoxylic acid, irrespective of production method (EI or CI), are identical, pointing to identical ion structures or mixture of structures. Fig. 1 (lower trace) shows one of these CID spectra. In addition to the H_3O^+ peak (*m/z* 19, loss of 2CO), the peak at *m/z* 29 (due to the combined losses of H_2O and CO), one at *m/z* 45 (loss of CH_2O) and *m/z* 46 (loss of HCO) are dominating. One should also notice the absence of a peak at *m/z* 47, that is, of the loss of CO giving protonated formic acid, and of a peak at *m/z* 31 that is, loss of CO_2 giving protonated formaldehyde.

The low vapour pressure of glyoxylic acid prevents its introduction via a leak valve into an ultrahigh vacuum chamber. Unfortunately, this eliminates the possibility for variable energy protonation experiments within an FT-ICR mass spectrometer.

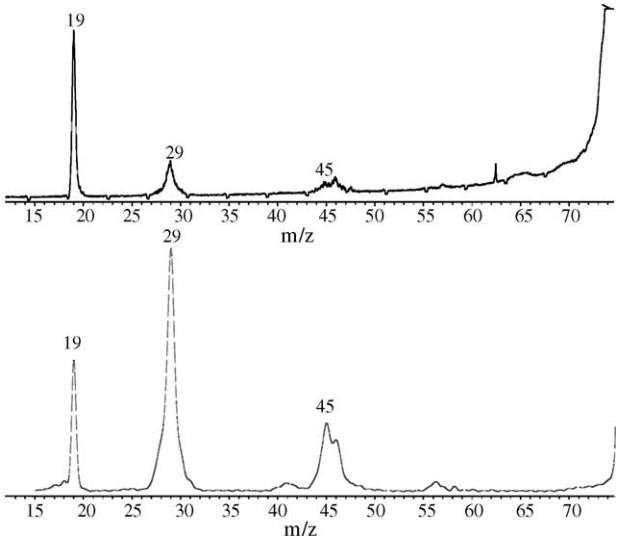

Fig. 1. MIKE and CID/MIKE spectra of ions $H_3C_2O_3^+$ (*m/z* 75). Upper trace: MIKES of protonated glyoxic acid (CI, H_2/CO). Lower trace: CID/MIKES of the $[M - CF_3]^+$ ions from trifluorolactic acid.

4.2. Potential energy surface

In order to reveal details of the unimolecular decomposition of protonated glyoxylic acid the relevant parts of the $[C_2, H_3, O_3]^+$ potential energy surface were mapped, first at the MP2/6–31 G(d,p) level of theory, thereafter using the G3 scheme for more accurate energy estimates. The resulting energy diagram is presented in Fig. 2, and structures are depicted in Fig. 3. The most stable tautomeric form of protonated glyoxylic acid is the result of protonation at the carbonyl oxygen of the carboxylic acid group, structure **1**. The proton affinity (PA) of glyoxylic acid, based on this lowest energy structure is estimated using G3 to be 745 kJ mol^{-1}. No experimental value is available for direct comparison. The accepted experimental value of formic acid is PA = 742 kJ mol^{-1} [22], which has been calculated by G2 to have PA = 744 kJ mol^{-1} [23]. A high potential energy barrier **TS(1′/7)** of 193.9 kJ mol^{-1} relative to **1** prevents direct dissociation of this isomer into the otherwise possible products $HC(OH)_2^+$ (*m/z* 47) + CO (Fig. 2). The thermochemically less stable combination HCOOH + HCO^+ (*m/z* 29) would be an alternative fragment pair produced via the same high energy TS. Tautomer **2**, corresponding to protonation of the aldehyde group is only 28.7 kJ mol^{-1} higher in potential energy than **1**. For both **1** and **2** there exists stereoisomers **1′** and **2′**, which are 29 and 13 kJ mol^{-1} less stable, respectively. Quite low potential energy barriers separate these four isomers as evident from Fig. 2. According to our model the highest critical point of the route to dissociation is via **TS(2′/3)**, that lies at 91.5 kJ mol^{-1} relative to **1**. The role of the corresponding transition structure is to accomplish transfer of the proton to the hydroxyl oxygen, to give **3**, thereby producing a molecule with a built-in water moiety. The barrier for direct conversion of **1** into **3**, **TS(1/3)** is at 216 kJ mol^{-1} (not included in Fig. 2).

In the following step of the transformation, the central carbonyl group is expelled as carbon monoxide. A potential energy minimum for **4** could be located, corresponding to complex between CO and hydroxyl-protonated formic acid (**5**). The latter has a C–O bond length of 1.743 Å MP2 (full)/6–31 G(d), and can be regarded as in-between a covalent structure and a complex between the formyl cation and water. This step is followed by intramolecular proton transfer, via **TS(5/6)** to give **6** which is a complex between the hydroxonium ion and carbon monoxide. Since the protonated glyoxylic molecule contains the OCCO structural unit, it could be a suitable precursor for the long-sought ethylenedione molecule. However, on the basis of the present energy diagram, we have to abandon that idea. Theoretical calculations by Talbi and Chandler [10] suggest that the triplet OCCO molecule is 246 kJ mol^{-1} above two separate CO molecules in potential energy. We, therefore, conclude that the two CO losses occur in sequence, rather than simultaneously, and quite certainly not in the form of an ethylenedione molecule [24–26]. It is also clear that dissociation to give the HCO^+ ion (**10**) would require 56.5 kJ mol^{-1} more than that of the critical **TS(2′/3)** (Fig. 2). It is unlikely that metastable ions will possess this much energy. Alternatively, a route much more energetically likely is loss of a water to give the hydrogen-bonded complex between a formyl cation and carbon monoxide, OC–$H^+\cdots$CO

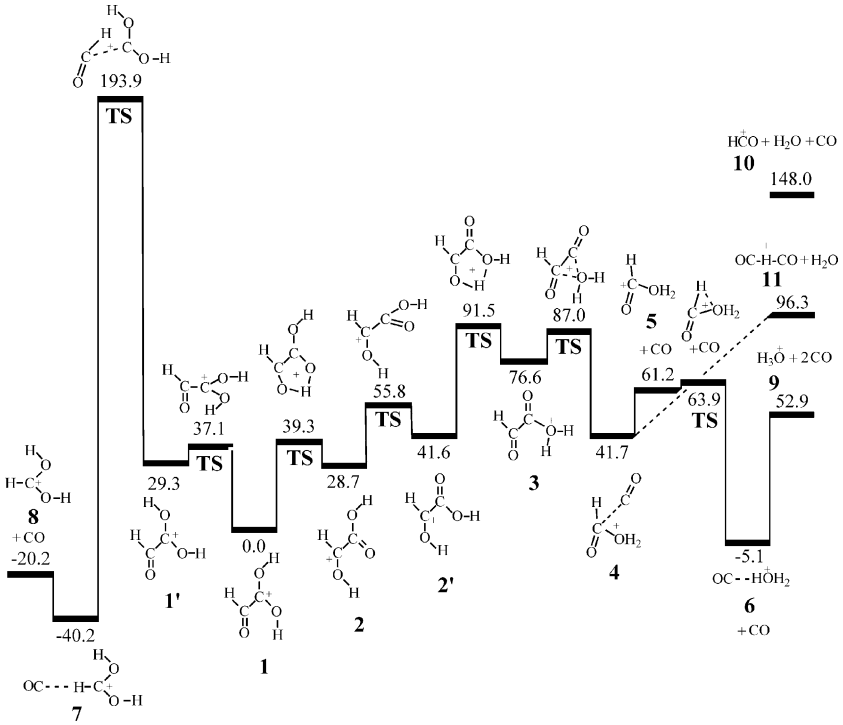

Fig. 2. Potential energy surface (kJ mol^{-1}) of the decomposition of protonated glyoxylic acid obtained with G3 (0 K). Stationary structures marked with fat full line. The potential energy of the optional products $HCO^+ + HCOOH$ is estimated to be 131 kJ mol^{-1} based on the diffence in proton affinity between formic acid and carbon monoxide.

(**11**). The potential energy of these products is only 4.8 kJ mol^{-1} above **TS(2′/3)** (Fig. 2), so it is not clear why there is no peak at *m/z* 57 in the MIKE spectrum. Only the lowest energy path, to give H_3O^+, seems to be followed to the very end.

4.3. Dynamics calculations

Although the ab initio mechanistic scheme is consistent with the experimental observations, there are still open questions, in particular the absence of OC–$H^+\cdots$CO in the MIKE spectrum. What is the role of the many intermediates, and what are their lifetimes? Is it even possible that some of the stages are circumvented, and are there alternative reaction paths to the ultimate products? It is also interesting that there is no peak for CO loss at *m/z* 47 in the MIKE spectrum, corresponding to one of the two tautomeric forms of protonated formic acid, or the more likely isomer $H_2OH^+\cdots$CO (**6**). To explore these interesting questions we conducted a limited number of ab initio reaction trajectory calculations. In order to provide reliable answers to the questions raised above, it was necessary to ensure that the topography of the potential energy surface is sufficiently accurately described by the chosen ab initio level. After considering different HF and B3LYP variants, we ended with MP2/6–31 G(d,p). From the calculations reported above we knew already that MP2/6–31 G(d,p) provides reasonably accurate topography compared to our "benchmark" G3, see Table 1.

The trajectories were initiated at the key transition structure **TS(2′/3)**, which is the rate determining barrier according to the ab initio calculations of Fig. 2. From this TS, all 10 trajectories were set out towards the shallow valley corresponding to the hydroxyl protonated glyoxylic acid, **3**. Two of the trajectories stayed in this region of the potential energy surfaces for an extended period of time. Most noticable is trajectory 5, which remained around **3** until the moment of cut-off, which was $t = 1618$ fs after initiation. Trajectory 10 ran in the same region

Table 1
Energies

Structure	G3 (0 K) energies		MP2/6–31 G(d.p) energies	
	Hartrees	Relative (kJ mol^{-1})	Hartrees	Relative (kJ mol^{-1})
1	−303.1973	0.0	−302.5211	0.0
TS(1/2)	−303.1824	39.3	−302.5083	33.6
2	−303.1864	28.7	−302.5104	28.1
TS(2/2′)	−303.1761	55.8	−302.4973	62.5
2′	−303.1815	41.6	−302.5055	41.0
TS(2′/3)	−303.1625	91.5	−302.4901	81.4
3	−303.1682	76.6	−302.4973	62.5
TS(3/4)	−303.1642	87.0	−302.4935	72.5
4	−303.1814	41.7	−302.5129	21.5
5 + CO	−303.1740	61.2	−302.5042	44.4
TS(5/6) + CO	−303.1730	63.9	−302.5023	49.3
6 + CO	−303.1993	−5.1	−302.5314	−27.1
9 + 2CO	−303.1772	52.9	−302.5053	41.4
10 + H_2O + CO	−303.1410	148.0	−302.4646	148.4
TS(1/1′)	−303.1832	37.1	−302.5054	41.3
1′	−303.1862	29.3	−302.5088	32.3
TS(1′/7)	−303.1235	193.9	−302.4463	196.4
7	−303.2127	−40.2	−302.5388	−46.5
8 + CO	−303.2050	−20.2	−302.5291	−21.0
11 + H_2O	−303.1607	96.3	−302.4890	84.3

for 180 fs, before re-crossing **TS(2′/3)**. Thereafter the trajectory ran in the local area around **2′** for 2250 fs. Subsequent bond rotation then led to **2**, and at $t = 2300$ fs the molecule isomerised into **1**, stayed in this form shortly until it re-isomerised to **2**, and then finally back to **1** at $t = 3100$ fs, and remained with this structure at cut-off at $t = 4837$ fs. This particular trajectory neatly illustrates the dynamic equilibrium between the four minimum energy structures at the reactant side of the rate-determining transition state. From Section 4.1, we recall that protonated glyoxylic acid made by CI gives an identical CID spectrum to the ion at *m/z* 75 in the EI spectrum of trifluorolactic acid. This resemblance could either be the result of one common ion structure or identical mixtures of isomers. The ab initio calculation, and in particular trajectory 10, give clear indication that the latter is the case (Table 2).

All remaining eight trajectories passed via **TS(3/4)** to accomodate liberation of one CO molecule. This event takes place in the range $t = 200$–300 fs. It is noticeable that the ejected CO remains in close contact to the remaining ionic entity for an extended period of time. In two cases, trajectories 6 and 8, we observed that the water moiety moved a bit away from the remaining molecule, increasing the contact to the carbon until around 2 Å. Thereafter, the formyl and the CO first remained in a situation where the C–C distance was less than 2 Å, until it

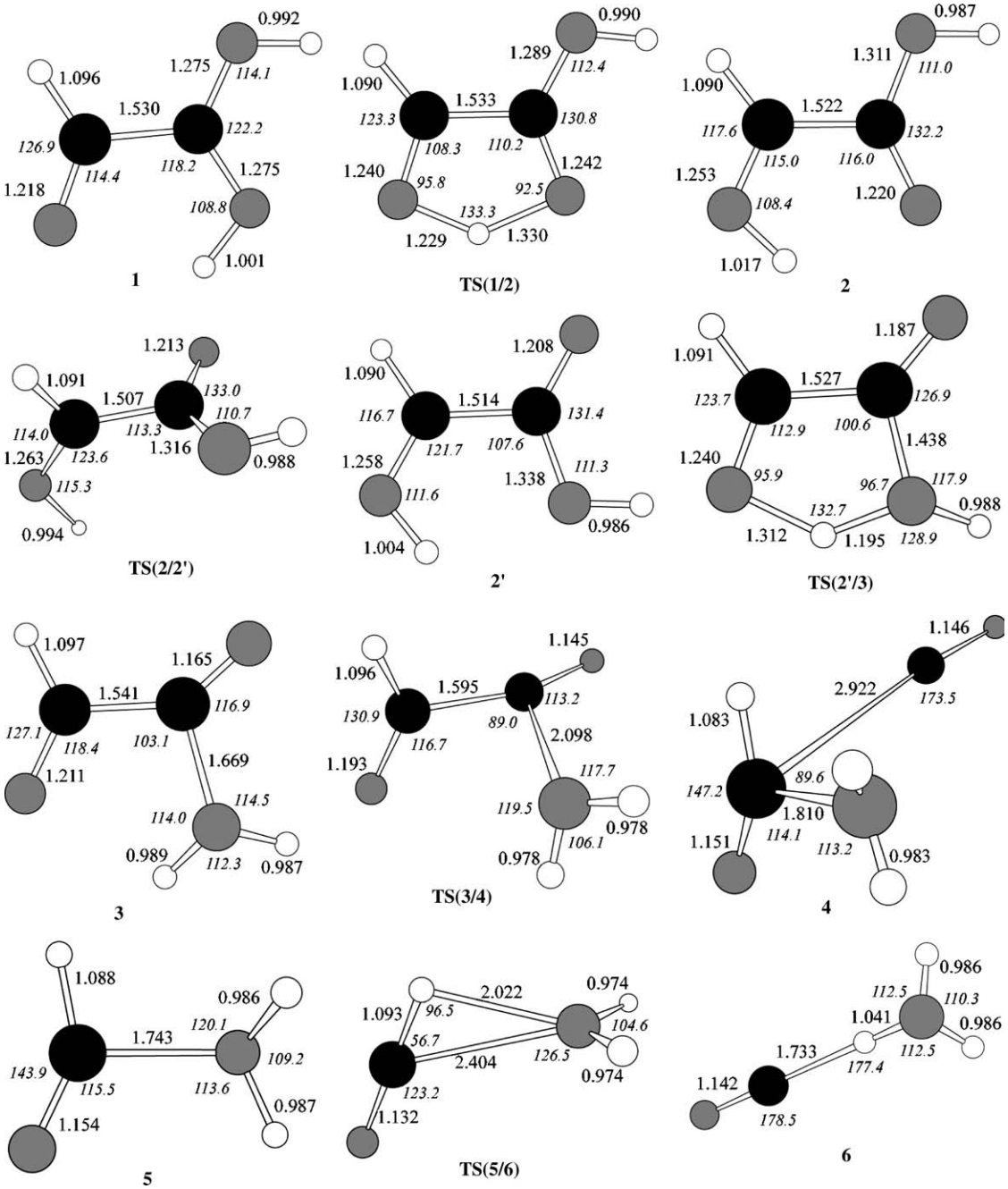

Fig. 3. Optimized structures at the MP2 (full)/6–31 G(d) level. Bond lengths are given in Å, and angles (italic) in degrees.

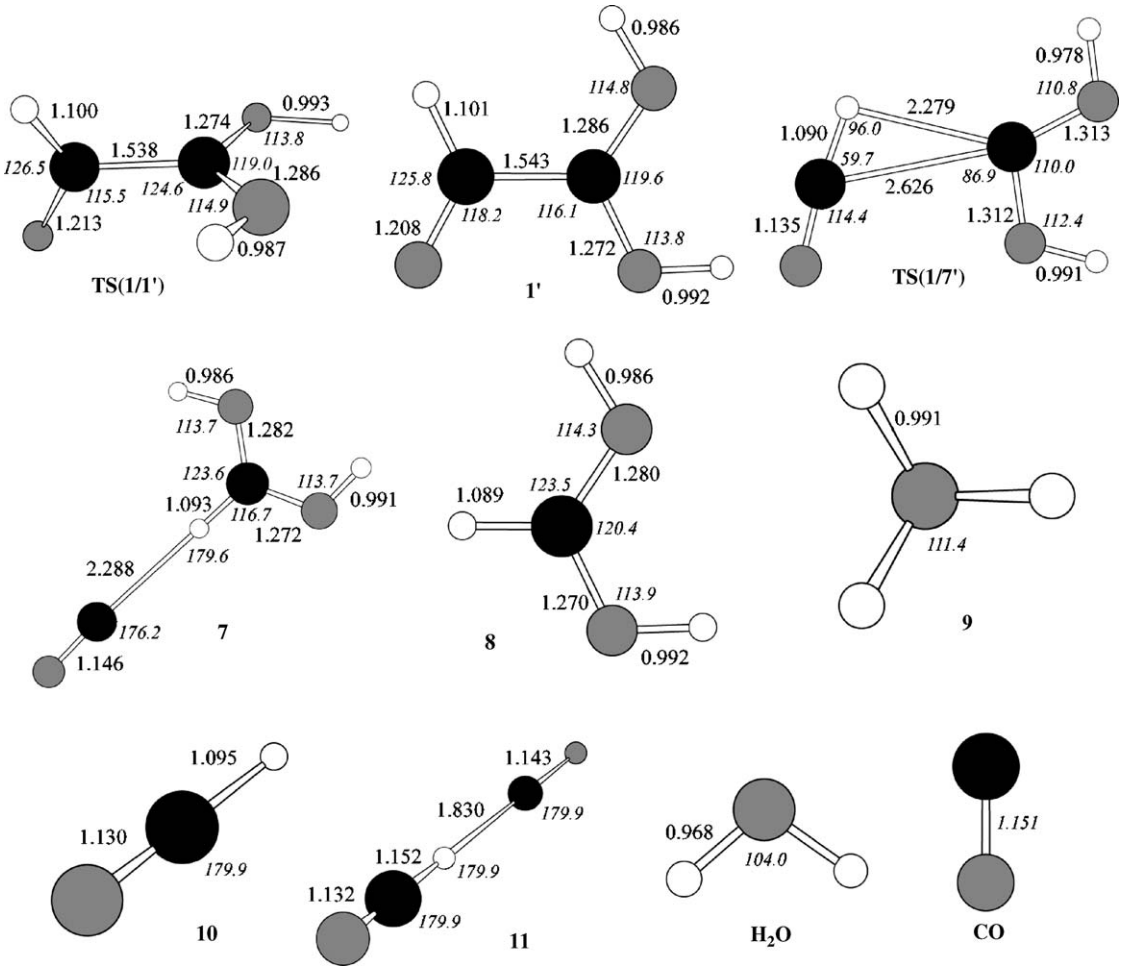

Fig. 3. (*Continued*).

slowly increased to ca. 2.2 Å. At this stage, the proton swung in-between the two carbons, and formed a transient OC–$H^+\cdots$CO structure. In both trajectories 6 and 8, the proton was about to transfer to the CO, but the attractive potential of the water molecule became too strong, and the proton moved over to the water oxygen atom, which then was roughly 1.5 Å perpendicular to the OC–$H^+\cdots$CO axis. The strategic position of the more basic water in this critical phase of the development explains why it picks up the proton, and that OC–$H^+\cdots$CO is not observed as a product in the MIKE spectrum.

Trajectories 1–4, 7 and 9 all left the valley around **4** and entered that of **5** in the time interval $t = 300$–500 fs. The three trajectories with the shortest cut-off times (1–3) ended up in this region at $t = 950$. The liberated CO remained within a distance of less than 10 Å while drifting slowly away. Even trajectory 7 which was integrated for the extended $t = 3040$ fs ended up to provide the $H_2OH^+\cdots$CO (**6**), with the other CO 41.4 Å away. It is noteworthy that only an extremely small fraction (a few percent) of the ions' excess energy ends up in vibrational, rotational and translational energy of the two CO molecules (the expelled

Table 2
Summary of reaction trajectories

Trajectory	No. of points	integrated time (fs)	Summary of the trajectory
1	950	915	→ **3** → **4** → **5** → $H_2OH^+\cdots$CO (**6**) + CO
2	950	916	→ **3** → **4** → **5** → $H_2OH^+\cdots$CO (**6**) + CO
3	950	886	→ **3** → **4** → **5** → $H_2OH^+\cdots$CO (**6**) + CO
4	1500	1283	→ **3** → **4** → **5** → $H_2OH^+\cdots$CO (**6**) + CO
5	1500	1618	→ H(CO)(CO)OH_2^+ (**3**)
6	1500	1370	→ **3** → **4** → **5** → **6** → H_3O^+ (**9**) + 2CO
7	3500	3040	→ **3** → **4** → **5** → $H_2OH^+\cdots$CO (**6**) + CO
8	6640	5883	→ **3** → **4** → **5** → **6** → H_3O^+ (**9**) + 2CO
9	6777	6104	→ **3** → **4** → **5** → **6** → H_3O^+ (**9**) + 2CO
10	5110	4837	→ **3** → **2′** → **2** → **1** → **2** → **1**

and the remaining). This is also evident from the animation, which shows vivid vibration within the newly formed H_3O^+ unit of **6**, especially in O–H stretching. It is therefore inevitable that, given sufficient time, $H_2OH^+\cdots CO$ will break up to give the free components. This is a key point. Trajectories 6, 8 and 9 show exactly this behaviour. In trajectory 6, the $H_2OH^+\cdots CO$ distance increases monotonously at the cut-off time ($t = 1370$) and the complexing hydrogen bond distance has reached a value of 5.2 Å. For trajectories 8 and 9, which had the longest integration times of 6 ps, complete dissociation was observed with the two CO molecules separated from the water by 43.5 and 54.1 Å, and 17.4 and 87.9 Å, respectively. The important observation is that on the product side of the critical transition state **TS(2′/3)**, breaking up $H_2OH^+\cdots CO$ (**6**) is the time demanding step. The rather inefficient coupling of intramolecular and intermolecular degrees of freedom sets the time the reacting molecular system have to spend in the valley around **6** to 1–2 ps; the latter is a strict downward limit, and some trajectories may run in the valley far longer.

The most significant outcome of the trajectory calculations is that it proves that our potential energy diagram in all aspects describes the essence of the reaction mechanism in how the only observed product H_3O^+ is formed. It is fascinating that the step-by-step mechanism envisaged from Fig. 2 indeed is followed, without any shortcuts, to product formation. The only small surprise is that the energetically accessible product ion $[OC\cdots HCO]^+$ (**11**, m/z 57) is not formed. Proton transfer to the strategically positioned water molecule formation observed in trajectories 6 and 8, efficiently disrupts its embryonic creation.

It is also significant that the no protonated formic acid is observed. The slow motion associated with the first expelled CO, allows for effective rearrangement into the more stable $H_3O^+\cdots CO$(**6**). As a result of this characteristics of the unimolecular reaction dynamics, no formation of HCO^+ is observed. This stands in stark contrast to the CID spectra, where HCO^+ is a major peak.

We have indicated that the principle of microscopic reversibility can be used as a guiding light for a retrosynthetic approach to the synthesis of molecules. At this point we know how protonated glyoxylic acid decomposes unimolecularly to give $H_3O^+ + 2CO$. Is it possible to turn this reaction upside down and make protonated glyoxylic acid in a gas-phase reaction between the hydroxonium ion and two molecules of carbon monoxide, for example, to mimic a reaction in the interstellar space? There are several favourable aspects. First of all, the overall reaction is highly exothermic. Secondly, the three product molecules were observed to drift slowly away from each other, rather than to explode apart. For the reverse reaction this is highly advantageous since there is little requirement for precise alignment of the molecules prior to reaction, or for the molecules to possess superthermal speeds. Thirdly, the step-by-step mechanism of the forward reaction opens up for a similar behaviour for the reverse route. On the other hand, for a gas-phase reaction with limited energy resources available, an uphill climb from separated $H_3O^+ + CO + CO$ molecules to **TS(2′/3)** could be prohibitive. In that sense it would be better to start with the proton bound dimer of two carbon monoxide molecules (**11**) plus water, since it is above **TS(2′/3)**. It would be even better with a larger cluster, in order to avoid the water only picking up the proton before leaving. In finalizing this discussion, we would like to point out that reaching **TS(3/4)** from the right-hand side could be sufficient for successful passage into the protonated glyoxylic acid region, since we have learned that there exist trajectories which cross **TS(2′/3)** from the right-hand side (Fig. 2).

5. Conclusion

In this work, we have established a detailed mechanism for how protonated glyoxylic acid $[HCOCOOH + H]^+$, decomposes to give one single ionic product, H_3O^+. The mechanism is based on experimental observations of the unimolecular reactivity studied by mass spectrometric methods in combination with high-level ab initio calculations. The mechanism is confirmed by direct dynamics calculations, which also demonstrates the importance of understanding the detailed atomic motions en route to products, and not only the details of the potential energy surface.

Acknowledgement

The authors wish to thank The Research Council of Norway (Programme for Supercomputing, NOTUR) for generous allocation of computer time to the project NN2386K.

References

[1] S. Beranová, J. Cai, C. Wesdemiotis, J. Am. Chem. Soc. 117 (1995) 9492.
[2] E. Uggerud, Theor. Chim. Acta 97 (1997) 313.
[3] B. Balta, M. Basma, V. Aviyente, C. Zhu, C. Lifshitz, Int. J. Mass Spectrom. 201 (2000) 69.
[4] R.A.J. O'Hair, P.S. Broughton, M.L. Styles, B.T. Frink, C.M. Hadad, J. Am. Soc. Mass Spectrom. 11 (2000) 687.
[5] R.D. Kinser, D.P. Ridge, G. Hvistendahl, B. Rasmussen, E. Uggerud, Chem. Eur. J. 2 (1996) 1143.
[6] H.Y. Lin, D.P. Ridge, T. Vulpius, E. Uggerud, J. Am. Chem. Soc. 116 (1994) 2996.
[7] O. Sekiguchi, V. Bakken, E. Uggerud, J. Am. Soc. Mass Spectrom. 15 (2004) 982.
[8] G.I. Mackay, A.C. Hopkinson, D.K. Bohme, J. Am. Chem. Soc. 100 (1978) 7460.
[9] D. Schröder, C. Heinemann, H. Schwarz, J.N. Harvey, S. Dua, S.J. Blanksby, J.H. Bowie, Chem. A: Eur. J. 4 (1998) 2550.
[10] D. Talbi, G.S. Chandler, J. Phys. Chem. A 104 (2000) 5872.
[11] D. Suelzle, T. Weiske, H. Schwarz, Int. J. Mass Spectrom. Ion Process. 125 (1993) 75.
[12] M.J. Frisch, G.W. Trucks, H.B. Schlegel, G.E. Scuseria, M.A. Robb, J.R. Cheeseman, J.A. Montgomery Jr., T. Vreven, K.N. Kudin, J.C. Burant, J.M. Millam, S.S. Iyengar, J. Tomasi, V. Barone, B. Mennucci, M. Cossi, G. Scalmani, N. Rega, G.A. Petersson, H. Nakatsuji, M. Hada, M. Ehara, K. Toyota, R. Fukuda, J. Hasegawa, M. Ishida, T. Nakajima, Y. Honda, O. Kitao, H. Nakai, M. Klene, X. Li, J.E. Knox, H.P. Hratchian, J.B. Cross, V. Bakken, C. Adamo, J. Jaramillo, R. Gomperts, R.E. Stratmann, O. Yazyev, A.J. Austin, R. Cammi, C. Pomelli, J.W. Ochterski, P.Y. Ayala, K. Morokuma, G.A. Voth, P. Salvador, J.J. Dannenberg, V.G. Zakrzewski, S. Dapprich, A.D. Daniels, M.C. Strain, O. Farkas, D.K. Malick, A.D. Rabuck, K. Raghavachari, J.B. Foresman, J.V. Ortiz, Q. Cui, A.G. Baboul, S. Clifford, J. Cioslowski, B.B. Stefanov, G. Liu, A. Liashenko, P. Piskorz, I. Komaromi, R.L. Martin, D.J. Fox, T. Keith,

M.A. Al-Laham, C.Y. Peng, A. Nanayakkara, M. Challacombe, P.M.W. Gill, B. Johnson, W. Chen, M.W. Wong, C. Gonzalez, J.A. Pople, Gaussian 03, Revision C.02, Gaussian Inc., Wallingford, CT, 2004.
[13] A.P. Scott, L. Radom, J. Phys. Chem. 100 (1996) 16502.
[14] C. Gonzales, H.B. Schlegel, J. Chem. Phys. 90 (1989) 2154.
[15] L.A. Curtiss, K. Raghavachari, G.W. Trucks, J.A. Pople, J. Chem. Phys. 94 (1991) 7221.
[16] T. Helgaker, E. Uggerud, H.J.A. Jensen, Chem. Phys. Lett. 173 (1990) 145.
[17] W. Chen, W.L. Hase, H.B. Schlegel, Chem. Phys. Lett. 228 (1994) 436.
[18] V. Bakken, J.M. Millam, H.B. Schlegel, J. Chem. Phys. 111 (1999) 8773.
[19] J.M. Millam, V. Bakken, W. Chen, W.L. Hase, H.B. Schlegel, J. Chem. Phys. 111 (1999) 3800.
[20] W.L. Hase, in: P.V.R. Schleyer, N.L. Allinger, T. Clark, J. Gasteiger, P.A. Kollmann, H.F. Schaefer III, P.R. Schreiner (Eds.), Encyclopedia of Computational Chemistry, Wiley, Chichester, 1998.
[21] S. Tajima, D. Watanabe, S. Nakajima, O. Sekiguchi, N.M.M. Nibbering, Int. J. Mass Spectrom. 207 (2001) 217.
[22] NIST Standard Reference Database Number 69, March 2003 Release, National Institute of Standards and Technology, Gaithersburg, MD 20899.
[23] B.J. Smith, L. Radom, J. Phys. Chem. 99 (1995) 6468.
[24] An interesting parallel to the sequential losses of two CO molecules from $[H(CO)COOH + H]^+$ ions (**1**) was found previously in the sequential elimination of two molecules of benzene from protonated oligophenylalkanes, occurring within the same field-free region of a sector-field mass spectrometer as well (cf. Refs. [25,26]).
[25] D. Kuck, A. Petersen, U. Fastabend, Int. J. Mass Spectrom. (179/180) (1998) 120.
[26] D. Kuck, A. Petersen, U. Fastabend, Int. J. Mass Spectrom. 179/180 (1998) 147.